Governing Role of Solvent on Discharge Activity in Lithium–CO_2 Batteries

Citation: Khurram, Aliza et al. "Governing Role of Solvent on Discharge Activity in Lithium–CO_2 Batteries." Journal of Physical Chemistry Letters, 10, 21 (November 2019): 6679-6687 © 2019 The Author(s)

As Published: 10.1021/ACS.JPCLETT.9B02615

Publisher: American Chemical Society (ACS)

Persistent URL: https://hdl.handle.net/1721.1/127776

Version: Author's final manuscript: final author's manuscript post peer review, without publisher's formatting or copy editing

Promoting Amine-Activated Electrochemical CO_2 Conversion with Alkali Salts

Aliza Khurram[1], Lifu Yan[2], Yuming Yin[2], Lingling Zhao[2], Betar M. Gallant[1*]

[1]Department of Mechanical Engineering, Massachusetts Institute of Technology, 77 Massachusetts Avenue, Cambridge, MA USA

[2]Key Laboratory of Energy Thermal Conversion and Control of Ministry of Education, School of Energy & Environment, Southeast University, Nanjing 210096, China

*Email: bgallant@mit.edu

ABSTRACT

Amine-based CO_2 chemisorption has been a longstanding motif under development for CO_2 capture applications, but large energy penalties are required to thermally cleave the N-C bond and regenerate CO_2 for subsequent storage or utilization. Instead, it is attractive to be able to directly perform electrochemical reactions on the amine solutions with loaded CO_2. We recently found that such a process is viable in dimethyl sulfoxide (DMSO) if an exogenous Li-based salt is present, leading to formation of CO_2-derived products through electrochemical N-C bond cleavage. However, the detailed influence of the salt on the electrochemical reactions was not understood. Here, we investigate the role of individual electrolyte salt constituents across multiple cations and anions in DMSO to gain improved insight into the salt's role in these complex electrolytes. While the anion appears to have minor effect, the cation is found to strongly modulate the thermochemistry of the amine-CO_2 through electrostatic interactions: ^{1}H NMR measurements show that post-capture, pre-reduction equilibrium proportions of the formed cation-associated carbamate vary by up to five-fold, and increase with the cation's Lewis acidity (e.g. from $K^+ \rightarrow Na^+ \rightarrow Li^+$). This trend is quantitatively supported by DFT calculations of the free energy of formation of these alkali-associated adducts. Upon electrochemical reduction, however, the current densities follow an opposing trend, with enhanced reaction rates obtained with the lowest Lewis-acidity cation, K^+. Meanwhile, molecular dynamics simulations indicate significant increases in desolvation and pairing kinetics that occur with K^+. These findings suggest that, in addition to strongly affecting the speciation of amine-CO_2 adducts, the cation's pairing with $–COO^-$ in the amine-CO_2 adduct can significantly hinder or enhance the rates of electrochemical reactions at moderate overpotentials. Consequently, designing electrolytes to

promote fast cation-transfer appears important for obtaining higher current densities in future systems.

Introduction

Carbon dioxide (CO_2) capture and utilization (CCU) is an attractive technology to address large scale CO_2 emissions from point sources such as power plants.[1-2] However, CCU generally requires significant energy inputs, both upstream - during capture and concentration of CO_2 at point of emission - and downstream, during subsequent reactions.[3-4] For example, capture of CO_2 from coal-fired plants, and its regeneration back to the gas phase, has been estimated to reduce the power output of the plant by up to 30%.[5-6] Meanwhile, electrochemical conversion - widely proposed as a method of downstream utilization of captured CO_2, with an objective of synthesizing chemicals or fuels - involves high overpotentials associated with water splitting[7-8] and the CO_2 reduction reaction,[9-10] further increasing energy requirements. Given these challenges, interest has been increasingly growing in combined capture-conversion processes that can directly utilize chemisorbed CO_2 as the reactant in a subsequent electrochemical process, obviating the need to regenerate CO_2 back to the gas phase.[11-14]

Utilizing chemisorbed CO_2 directly, rather than post-separation CO_2, invites design of new classes of electrochemical reactions by relaxing some of the key constraints of classical CO_2 electroreduction.[15] Given the high overpotentials required for the latter (e.g., > 1 V for CH_4 on Cu electrocatalysts)[16], emphasis has largely been placed on lowering the free energy barrier of the reduction intermediate, the CO_2 anion ("CO_2^-"). This is typically accomplished through design of the electrode (catalyst) material, which can lower kinetic barriers by promoting stabilization of this high-energy species. However, significantly less attention has been devoted to modifying the *reactant* state of CO_2 as a means to potentially improve conversion kinetics, for example by chemically incorporating CO_2 into an adduct. Ideally, this species would be capable of subsequent electrochemical reactions that induce detachment of "CO_2" (or a reduced CO_2 anion intermediate), enabling its subsequent reactivity with electrons and cations,[17] while the agent used to bind the CO_2 can be re-used for further reactions. If successful, such a scheme could obviate the need for energetically-intensive CO_2 release and separation between the capture and utilization steps. Realizing such a combined capture-conversion approach, however,

requires a substrate with a CO_2 binding strength that is neither too strong (impractically stabilizing the "CO_2") nor too weak. Amines, a motif abundantly studied in literature for promoting CO_2 chemical interactions, are promising in this regard due to their moderate chemisorption of CO_2 (-65 to -80 kJ/mol CO_2) in both aqueous[18-19] and nonaqueous media,[20-21] which has been widely exploited for applications in CO_2 capture.[5, 22-24] In those applications, CO_2 is typically regenerated by thermally-induced N-C bond cleavage at elevated temperatures (e.g. 100 – 120 °C),[22] followed by compression for long-term storage or downstream utilization. Until recently, however, it has remained an open question whether amines can be utilized to promote direct electrochemical reactions.

Table 1: Integrated chemical capture and electrochemical conversion of CO_2 in a DMSO-based electrolyte containing Li^+-salt.

CO_2 capture in neat DMSO:	$2RNH_2 + 2CO_2 \rightarrow 2RNHCOOH$	(1)
Salt-induced re-speciation:	$2RNHCOOH + Li^+ \rightarrow RNHCOO^-Li^+ + RNH_3^+ + CO_2$	(2)
Net capture step:	$2RNH_2 + CO_2 + Li^+ \rightarrow RNHCOO^-Li^+ + RNH_3^+$	(3)
Electrochemical conversion step:	$RNHCOO^-Li^+ + RNH_3^+ + 2CO_2 + 3Li^+ + 4e^- \rightarrow 2Li_2CO_3 + C + 2RNH_2$	(4)
Net capture-conversion reaction:	$3CO_2 + 4Li^+ + 4e^- \rightarrow 2Li_2CO_3 + C$	(5)

Recently, we reported that such a scheme is possible**.** We studied chemisorption of CO_2 by an alkylamine, 2-ethoxyethylamine (EEA), in dimethylsulfoxide (DMSO) with an exogenous Li^+-based co-salt. In neat DMSO (no co-salt), CO_2 uptake by EEA resulted in the preferential formation of carbamic acid (Reaction 1 in **Table 1**). Subsequent inclusion of the salt, however, induced conversion of all carbamic acid to lithium carbamate (Reaction 2). We found that the lithium carbamate, and not the carbamic acid, was intrinsically electroactive, exhibiting reduction activity at high potentials of ~2.8 V vs. Li/Li^+. Meanwhile, physisorbed CO_2 exhibited no electroactivity in the same DMSO electrolyte without the amine.[25] Upon electron transfer, the carbamate species were found to undergo selective N-C bond cleavage, with the resulting products (predominantly Li_2CO_3) consisting of only CO_2-derived species. Meanwhile, the amine remained in solution, capable of further CO_2 uptake. The overall electrochemical reaction

occurred according to Reaction 4, in which the amine-bound CO_2, as $RNHCOO^-$, played the central role as the electroactive species (**Figure 1**). Our results suggested that the product lean amine ($2RNH_2$) could undergo limited turnovers (<10) by re-binding CO_2, yet ultimately became deactivated, likely due to side reactions at the Li electrode.

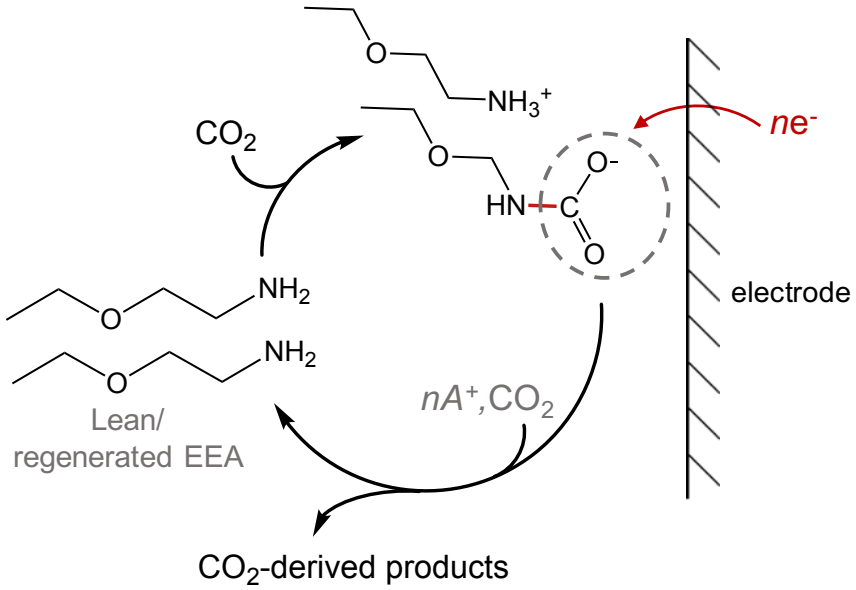

Figure 1: Electrochemical reduction scheme of the CO_2 conversion pathway via selective cleavage of the N-C bond (A^+ = alkali cation).

In that first work, the feasibility of electrochemical, amine-based CO_2 conversion was investigated in nonaqueous electrolyte to simplify and isolate the conversion reaction for easier interrogation. This is otherwise substantially more challenging in aqueous solutions, given the combined proton lability during capture and conversion, possible participation of H_2O in the electrochemical reactions, and the difficulty in detecting potential liquid products, likely at low concentrations, which may have overlapping spectroscopic signatures with the amine. Use of nonaqueous electrolytes limits the available conversion products to solid carbonates and carbon, but opens new opportunities for design of both energy storage and sequestration reactions.[26-27] For example, Li_2CO_3 is the principal discharge product in primary or rechargeable Li-CO_2 batteries that utilize post-separation CO_2 as the gas cathode, but it is presently unclear how to couple CO_2 emissions into the cell without accruing the large regeneration penalties from upstream capture. Combined capture-conversion approaches may provide this critical link. In addition, capture-conversion may be used to develop future electrochemically-driven processes

that accelerate sequestration of CO_2 in safe, disposable alkali or alkaline-earth carbonates, which could relieve dependence on underground storage of compressed CO_2. Regardless of the eventual application, a nonaqueous environment provides a valuable model system for exploring the viability of selective electrochemical N-C bond cleavage, an essential first step to determine whether subsequent investigations in a wider range of media could be deemed worthwhile. As our first study used a single electrolyte composition (solvent, salt, and amine), it remained unknown whether amine-facilitated CO_2 conversion is generalizable, as might be expected, to other alkali cations, nor the specific role of the electrolyte salt (cation and anion), which could affect both the reactant-state populations and the subsequent electrochemical kinetics.

In this work, the detailed role played by the electrolyte salt is examined. First, modifications in the amine-CO_2 speciation (post-capture, pre-reduction) in the presence of alkali salts are monitored by *ex situ* ^{1}H NMR spectroscopy for a range of co-salt anions (ClO_4^-, PF_6^-, and $TFSI^-$) and cations (Li^+, Na^+, K^+, and TBA^+). A strong correlation is found between the cation's Lewis acidity and the population of formed carbamate. Density functional theory (DFT) calculations support this correlation by quantitatively comparing the free energy and enthalpy changes during the approach to chemical equilibrium. While DFT calculations provide valuable insights into the captured-state (and thus the electrochemical reactant-state) thermodynamics and geometries, they cannot capture the dynamics of systems actively undergoing electrochemical reactions. Therefore, to unify the reactant-state thermodynamics and the subsequent electrochemical reaction rates, the role of ion transport and desolvation kinetics are probed using molecular dynamics (MD) simulations. In conjunction, these efforts reveal the significance of the identity of the electrolyte co-salt cation and its solvation structure on modulating the electrochemical activity of amine-CO_2 adducts. Moreover, our results provide guidelines to increase the rates of amine-CO_2 electrochemical reactions in future work through the design of electrolytes in which cations are less-strongly solvated.

Experimental Methods

Cyclic voltammetry (CV) measurements

Cyclic voltammetry (CV) measurements were conducted inside the argon glovebox using a 3-electrode electrolysis-type cell containing a fritted Pt counter electrode, a fritted, nonaqueous

$AgNO_3$ reference electrode (Ag wire immersed in 0.1 M $TBAClO_4$ / 0.01 M $AgNO_3$ in acetonitrile), and a carbon Super-P coated glassy carbon (GC, Pine, A = 0.196 cm^2, typical Super-P loading of 2.01 ± 0.05 mg) mounted to a Modulated Speed Rotator (Pine) working electrode. The reference electrode potential was typically found to scale as 0 V_{Li} ~ -3.62 V vs. Ag/Ag^+ (further details in Supporting Information). For simplicity, in the main text, only the negative-going sweep is shown (linear sweep voltammetry).

Spectroscopy measurements

Attenuated total reflectance infrared (ATR-IR) spectroscopy measurements were performed using a Nicolet 6700 spectrometer (Thermo Scientific) with a zinc selenide crystal in transmission mode over a wavenumber range of 650 to 4000 cm^{-1}. ^1H NMR measurements on solutions of anhydrous DMSO-d_6 (Sigma Aldrich) was performed using a Varian Inova 500 MHz NMR spectrometer equipped with dual broadband radio frequency and a 5-mm variable temperature switchable PFG probe. CO_2 loading of electrolytes was determined using mass spectrometry (MS Thermofisher GC-Q Exactive) following an acid treatment reported previously.[28] Samples were sealed under Ar, then injected with 85% H_3PO_4 under shaking incubation to evolve all of the chemically-bound CO_2. The sample was then injected with 85% H_3PO_4 twice more to confirm that all CO_2 had been released.

Computational methods

DFT simulations were carried out using Gaussian Software. For each individual species (RNH_2, alkali-metal cation, DMSO, carbamic acid, carbamate, and ammonium), structure optimizations were conducted separately to obtain stable equilibrium configurations. Geometry minimization was calculated at the B3LYP/6-311++G(d, p) level of theory.[29] All simulations used the Solvation Model Based on Density (SMD) to account for the solvent dielectric constant (ϵ_{DMSO}).[30] Optimized structures were confirmed by vibration frequency calculations at the B3LPY/6-311++G(d, p) level of theory. Zero-point energy, thermal correction to the enthalpy and the solute free energy (i.e. free energy of vacuum plus the solvation free energy) for each species were computed at 298 K. Molecular Dynamics (MD) simulations were performed by the GROMACS 5.1.2 software package.[31] Both bonded and nonbonded interactions were considered. Nonbonded interactions, which involve van der Waals (vdW) and electrostatic

interactions, were calculated by the Lennard-Jones (LJ) potential and Coulomb's law respectively, with a cutoff distance of 12 Å. Bond stretching and O-C-O angle were modeled using a harmonic potential energy function, and bonded dihedral interactions were calculated with the Ryckaert-Bellemans function. The all-atoms flexible DMSO model[32] was used to model DMSO. Meanwhile, $RNHCOO^-$ and cations (i.e. Li^+, Na^+, and K^+) were simulated by the OPLS-AA force field flexible model.[33] Additional information is available in the SI.

Results and Discussion

Equilibrium speciation of CO_2-loaded EEA with varying salt compositions in DMSO

Our previous study investigated electrochemical performance with EEA in DMSO and $LiClO_4$ as the co-salt.[25] Here, we utilize the same solvent, amine, and concentration (0.1 M EEA) while varying the electrolyte co-salt constituents. We first investigated the influence of salt on the equilibrium speciation of the amine-CO_2 adduct. In non-aqueous solvents, CO_2 uptake by primary amines proceeds through the formation of a zwitterion intermediate ($RNH_2^+COO^-$), which then follows one of two pathways depending on the solvent: the zwitterion proton can undergo an intramolecular proton transfer to form a stable carbamic acid (RNHCOOH, resulting loading: 1 mol CO_2/1 mol EEA). Alternatively, the zwitterion and/or carbamic acid can be deprotonated by a neighboring lean amine, yielding a carbamate anion ($RNHCOO^-$) and an ammonium cation (RNH_3^+, resulting loading: 0.5 mol CO_2/1 mol EEA, **Figure S1**).[34] As reported previously,[25] neat DMSO preferentially stabilized CO_2-loaded EEA in carbamic acid form with nearly 100% selectivity. The subsequent addition of a Li^+-containing salt, however, induced key shifts in equilibrium speciation, from predominantly carbamic acid to predominantly (deprotonated) lithium carbamate, with associated Li^+ in place of the acidic proton ($2RNHCOOH + Li^+ \rightarrow RNHCOO^-Li^+ + RNH_3^+ + CO_2$) . Displacement of the proton resulted in the formation of an accompanying ammonium cation from a nearby carbamic acid and the concurrent release of a bound CO_2 (**Figure 2**). The ammonium cation may then associate with a weakly coordinating co-salt anion, Y^-, forming $RNH_3^+Y^-$. Electrochemical measurements revealed that Li carbamate was intrinsically electrochemically active, and could be subsequently reduced at a carbon electrode to yield CO_2-derived products (predominantly Li_2CO_3).[25]

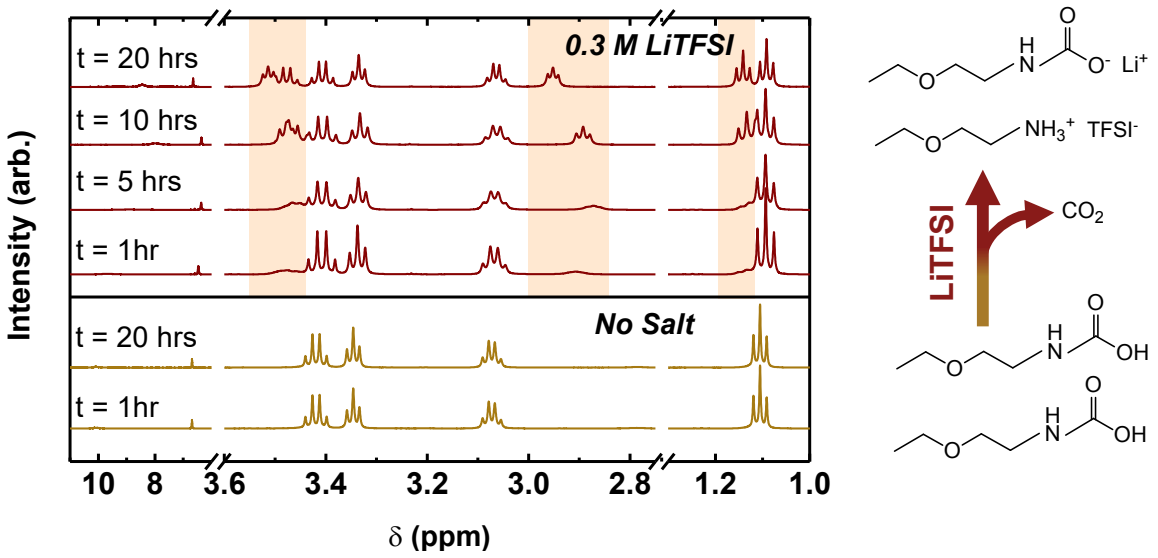

Figure 2: ^{1}H NMR spectra of DMSO-d_6 containing 0.1 M EEA-CO_2 prior to, and one hour, 5 hours, 10 hours, and 20 hours after addition of 0.3 M LiTFSI. The highlighted features in the NMR spectra show the ^{1}H resonances corresponding to the ammonium cation that emerge post-alkali salt addition.

Here, we began by investigating the salt's detailed influence on the equilibrium speciation of the EEA-CO_2 adducts for a range of different salt anions and cations. Aliquots of 0.1 M EEA-CO_2/DMSO, without and with 0.3 M salt, were taken at fixed time intervals post-salt addition for ^{1}H NMR analysis. Note that introducing the electrolyte salt prior to, or post-CO_2 introduction does not alter the equilibrium speciation of the adducts nor the kinetics of the reaction, but it was experimentally preferable to add the salt second in these measurements to ensure an equivalent initial amount of bound EEA-CO_2 before the initiation of any reaction.[25] As a control measurement, in the absence of added salt, the percentage of EEA-CO_2 adducts in carbamic acid form, as calculated[34] from the ^{1}H NMR spectra, remained stable at 99% over the course of several days **(Figure S2).** In contrast, comparable data taken with 0.3 M LiTFSI as the co-salt exhibited a slow shift in speciation of EEA-CO_2 adducts, evidenced by the emergence and growing intensity of spectral features at 1.15 ppm, 2.90 ppm, and 3.45 ppm **(Figure 2)**. These peaks indicate formation of the ammonium cation, which also implies proportional formation of carbamate (Reaction 2).[25] With LiTFSI, the percentage of EEA-CO_2 adducts existing as carbamate at one, five, 10 and 20 hours post-salt addition was calculated as 13.1%, 24.0%, 41.1% and 49.2%, respectively, of the total initial lean EEA concentration. Note that the maximum possible loading of carbamate is 50%, owing to the need to form an equimolar amount

of ammonium by Li^+-induced proton displacement; therefore, the conversion was nearly complete after 20 hours. Further sampling at 48 or 96 hours indicated negligible further changes (**Figure S3**). Unlike the relatively shorter timescales (order of several hours) associated with complete carbamate formation in aqueous CO_2 capture,[35] longer timescales observed in this work indicate that Li^+-driven carbamic acid-to-carbamate conversion is exceedingly sluggish at room temperature, and may be further exacerbated by the currently non-optimized properties of these atypical electrolytes combining amines, inorganic salts and DMSO. Although the rate-limiting factors of this complex, multi-bodied process are currently unknown, we hypothesize that this may be attributed to sluggish deprotonation of the carbamic acid to form a high-energy zwitterion intermediate prior to proton transfer to a neighboring amine,[36] and/or the relatively low concentrations and mobility of amines, making reaction events (requiring participation of two amines and a salt cation) relatively unlikely.

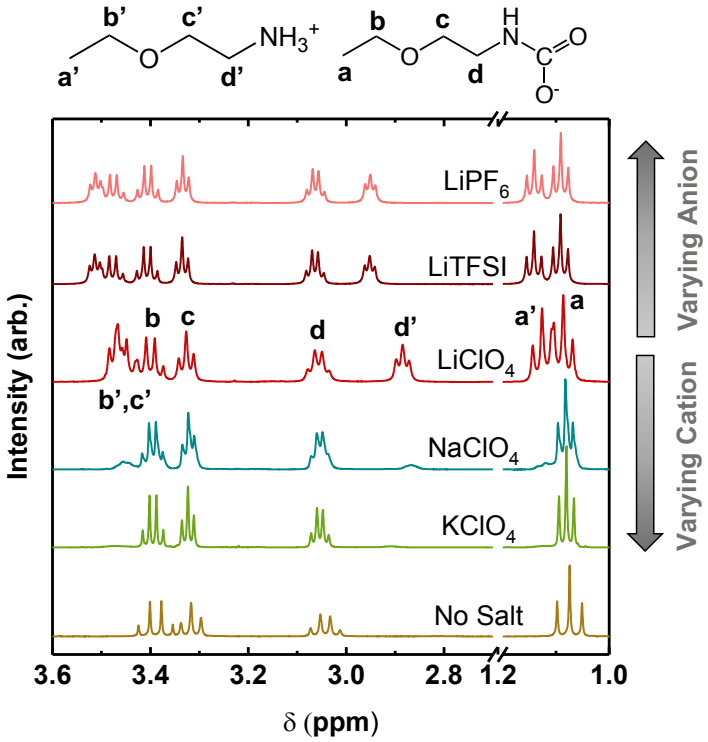

Figure 3: (a) ^{1}H NMR of DMSO-d_6 electrolyte containing 0.1 M EEA-CO_2, taken 20 hours after the addition of 0.3 M LiY/DMSO (Y^- = ClO_4^-, PF_6^-, or $TFSI^-$) or 0.3 M $AClO_4$ (A^+ = Li^+, Na^+, K^+).

The above analysis was next extended to include five additional co-salt compositions ($LiPF_6$, $LiClO_4$, $NaClO_4$, $KClO_4$, and $TBAClO_4$) to independently investigate the role of the co-salt cation or anion on the re-speciation process. **Figure 3** shows the ^1H NMR spectra for the aforementioned salts 20 hours after salt addition, and **Figure 4** summarizes the time-dependent variation in cation-associated carbamate populations for each case. The co-salt anion was found to have a very minor effect; 96 hours after salt addition, the equilibrium proportions of carbamate were found to be identical, within measurement error, at 49.5%, 49.8%, and 50.0% for ClO_4^-, PF_6^- and $TFSI^-$, respectively. Moreover, the rate of Li carbamate formation was also similar (time-dependent spectra for $LiClO_4$ and $LiPF_6$ are shown in **Figure S4**). Note that the chemical shifts of the peaks corresponding to the ammonium cation (indicated by a', b', c' and d' in **Figure 3**)[25,37] are slightly different for the three anions studied, likely due to varying strengths of ionic association between the ammonium cation and the co-salt anion, though the integrated intensities, reflecting the relative amounts, are similar.[25] Overall, these results show that the anion has little effect on the speciation of carbamic acid to Li^+-associated carbamate, and is not the main driver of this change in population.

In contrast to negligible effect of the anion, the cation was found to strongly influence the equilibrium populations of carbamate. Identical time-dependent ^1H NMR measurements were performed on EEA-CO_2 solutions containing perchlorate-based salt, 0.3 M $ACl O_4$, where A^+ = Li^+, Na^+, K^+ or TBA^+. As shown in **Figure 4** and **S5**, the quantity of formed ammonium cations decreased monotonically with decreasing Lewis acidity of the cations, in the order $Li^+ > Na^+ > K^+ > TBA^+$. The final equilibrium proportion of alkali carbamate formed 96 hours after salt addition was determined to vary by nearly a factor of five depending on the alkali cation alone, yielding 49.5%, 32.1%, and 11.3% carbamate for Li^+, Na^+, and K^+, respectively. Unexpectedly, a small amount of carbamate (7.4%) formed even with TBA^+, indicating a non-negligible, yet very weak, carbamate-TBA^+ interaction (the TBA^+ spectrum is omitted from **Figure 3** due to large background ^1H resonances, but time-dependent spectra are provided in **Figure S5**). These results clearly indicate that Li^+ associates most strongly with the initial carbamic acid, driving the conversion reaction to carbamate farthest to the right in DMSO. We could also separately confirm this trend in the NMR spectra, namely that solutions containing stronger Lewis acids corresponded to lower CO_2 loadings and thus higher carbamate proportions, by directly measuring the amount of CO_2 bound to EEA in the different equilibrated solutions. This was

accomplished by treating CO_2-rich electrolytes with 2 M H_3PO_4,[28] which released all chemically-bound CO_2 back to the gas phase where it was quantified via mass spectrometry. As shown in **Figure S6**, the CO_2 loading ratios for Li^+ and K^+, twenty hours after the addition of the salt, were 0.58 and 0.77 CO_2 per EEA, respectively (theoretical loading ratios are 0.5 for purely carbamate and 1 for purely carbamic acid), in good agreement with ^1H NMR spectra results. Note that the presence of trace water, potentially due to variations in different water contents of salts, could be ruled out as the origin of varying equilibrium proportions of carbamate, as water content in each of the as-prepared solutions was found to be negligible (<25 ppm, **Table S1**), especially compared to the 100 mM concentration of amines.

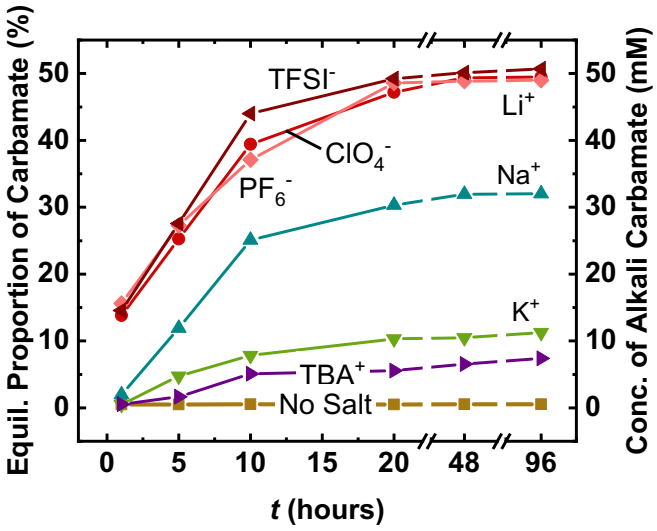

Figure 4: Equilibrium proportion and concentration of alkali or TBA carbamate, as determined by ^1H NMR in Figures 2 and S2-5, as a function of time after salt addition. The top three data sets correspond to the Li^+ cation with either $TFSI^-$, PF_6^- or ClO_4^- anions, whereas all other cations (Na^+, K^+, TBA^+) have ClO_4^- as the anion.

To glean further insight into the cation's role in driving carbamate formation, DFT calculations were conducted to extract the overall Gibbs free energy change during Reaction 2 ($2RNHCOOH + Li^+ \rightarrow RNHCOO^-Li^+ + RNH_3^+ + CO_2$) as a function of cation. Given the electrochemical activity of the alkali carbamate (-COOA), descriptors of the electronic structure changes and energetic driving forces during the re-speciation process are valuable to rationalize and parametrize the origins of emergent activity when electrochemistry is later conducted on the equilibrated solutions. First, the overall free energy change associated with the carbamic acid-to-

carbamate exchange was calculated for each of the three alkali cations. Systems consisting of two carbamic acid molecules (RNHCOOH) and one alkali cation were constructed. Geometry minimization and frequency calculations were run separately for the reactants (RNHCOOH and A^+) and products ($RNHCOO^-A^+$, RNH_3^+ and CO_2) at the B3LYP/6-311++G(d, p) level of theory[38] **(Figure 5a)**. Owing to computational constraints, solvation effects were treated implicitly using the Solvation Model Based on Density (SMD) to account for the solvent dielectric constant. As shown in **Figure 5b**, in the absence of an electrolyte co-salt, deprotonation of two carbamic acid molecules to form ammonium carbamate and a free CO_2 ($2RNHCOOH \rightarrow RNHCOO^- + RNH_3^+ + CO_2$) cannot spontaneously occur ($\Delta G_r = 2.5$ kJ/mol). The addition of alkali cations to this system, however, significantly altered the thermodynamic landscape. In the presence of Li^+, carbamic acid-to-carbamate conversion, concurrent with ion association between the Li^+ and the carbamate anion, occurs spontaneously with a large negative free energy change of $\Delta G_r = -143.1$ kJ/mol. Na^+ and K^+ also induced deprotonation of the carbamic acid to form the corresponding alkali carbamate, which, while still spontaneous, were less thermodynamically downhill ($\Delta G_r = -111.8$ kJ/mol and $\Delta G_r = -85.7$ kJ/mol for Na^+ and K^+, respectively). These findings are in good agreement with the experimental trends, where the population of carbamate decreased in the order of $Li^+ > Na^+ > K^+$, as smaller Gibbs free energy changes would favor lower populations of the product carbamate. In addition, the computed enthalpies of reaction, ΔH_r, which range from -133.3 kJ/mol (Li^+) to -73.2 kJ/mol (K^+), agree well with experimental values of alkyl amines measured elsewhere in aprotic solvents without added co-salts.[20] Overall, these results highlight the central role of the alkali cations in driving key shifts in equilibrium speciation of the EEA-CO_2 adducts which are necessary for the subsequent electrochemical activity to be observed.

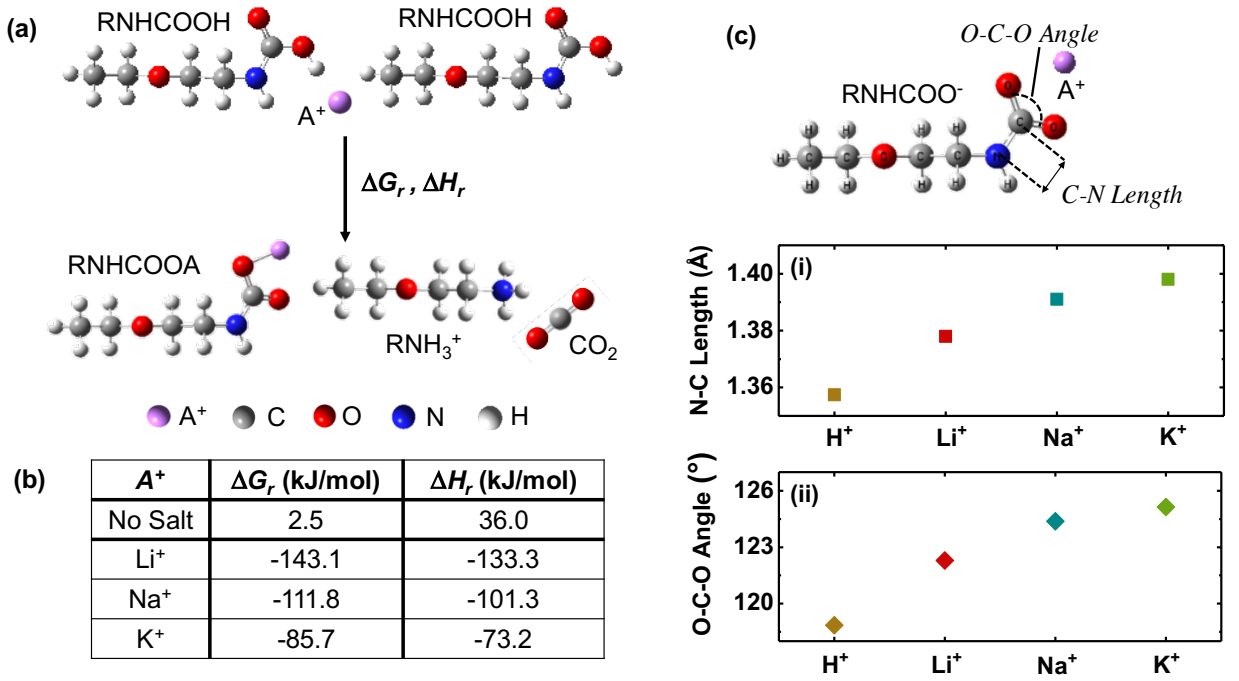

(b)

A^+	ΔG_r (kJ/mol)	ΔH_r (kJ/mol)
No Salt	2.5	36.0
Li^+	-143.1	-133.3
Na^+	-111.8	-101.3
K^+	-85.7	-73.2

Figure 5: (a) Optimized structures of RNHCOOH and A^+ (reactants) and $RNHCOO^-A^+$, RNH_3^+, and CO_2 (products) obtained via DFT post-geometry minimization (A^+ = Li^+, Na^+, or K^+). (b) Free energy (ΔG_r) and enthalpy (ΔH_r) differences incurred upon $2RNHCOOH + A^+ \rightarrow RNHCOO^-A^+ + RNH_3^+ + CO_2$. All enthalpy and free energy calculations were performed at T = 298 K and P_{CO2} = 1 atm. (c) N-C bond lengths and O-C-O bond angles in carbamic acid (RNHCOOH) and alkali metal carbamates.

The resulting N-C bond lengths and O-C-O bond angles were also found to vary significantly across the different alkali carbamates. As shown in **Figure 5c**, as electrostatic interactions decreased from Li^+ to K^+, the N-C bond lengthened monotonically from 1.38 to 1.40 Å, indicating N-C bond weakening with larger cation size. Carbamic acid (-COOH) possessed the shortest N-C bond length (1.50% shorter than in Li carbamate), and therefore the strongest N-C bond. This suggests that in comparison to alkali carbamates, neutral carbamic acid (more stable) is more difficult to electrochemically reduce via selective cleavage of the N-C bond than the alkali carbamate in solutions where both populations exist, favoring selective reduction of the latter. For alkali carbamates, the cation-dependent trend in N-C bond shortening is attributable to higher inductive effects around the terminal –COO for harder Lewis acids (e.g. Li^+), resulting in lower electron density around the carboxylate carbon and bond strengthening. Correspondingly, the O-C-O bond angle in the adduct varied proportionally, with smaller O-C-O bond angles (more "bent") for stronger Lewis acids (122.3° vs 125.1° for Li^+ or K^+, respectively) and shorter

N-C bond lengths. The trend of N-C bond strengthening with harder Lewis acids could also be experimentally validated by ATR-IR experiments performed with 1.5 M CO_2-loaded EEA and 2 M $LiClO_4$ (concentrations were proportionally increased to accentuate the relatively weak sensitivity of N-C stretches in IR measurements). As shown in **Figure S7**, consistent with the DFT calculations, the N-COO^- stretching vibration shifted from a higher wavenumber for Li carbamate (~1321 cm^{-1}), to lower wavenumbers for Na (~1311 cm^{-1}) and K (~ 1309 cm^{-1}) carbamate. Moreover, the characteristic carbamate peaks at 1576 and 1494 cm^{-1}, and the stretching vibration of N-COO^- at 1321 cm^{-1},[39-41] are strongest in overall intensity for Li^+ and decrease monotonically thereafter for Na^+ and K^+, consistent with maximum carbamate formation with Li^+.

DFT calculations also enabled interrogation of the LUMO structure in the alkali-associated carbamates, which indicate a significant degree of localization over the carbamate/cation moiety with little contribution from the alkyl ethoxy backbone **(Figure S8)**. This suggests that under subsequent electrochemical conditions, the first elementary electron transfer step results in added electron density centered generally around the N-C bond, yet delocalized somewhat over the -N-COO^-A^+ terminal end. Meanwhile, the backbone, i.e. $CH_3CH_2OCH_2CH_2$-, is expected from these calculations to be relatively unaffected, and therefore stable, upon electron transfer. We further investigated the change in electronic structure of lithium carbamate upon the addition of a single electron to predict changes that may occur under electrochemical conditions. While the bond length changes are generally an order of magnitude larger for the bonds in the $NCOO^-$ termination than they are for those in the alkyl ethoxy tail of the amine **(Figure S9)**, the overall changes were relatively minor (< 2%) for the N-C and C-O bonds, respectively. This suggests that although these bonds are most significantly weakened upon reduction, the reduced form of the adduct may remain relatively stable for subsequent ion transfer, electron transfer, and/or reaction with additional CO_2[42] before the N-C bond cleavage event occurs.

Effect of electrolyte salt on the electrochemical activity of CO_2-loaded EEA

Having characterized the electrochemical reactant state in detail, we next studied how the salt constituents influence the subsequent electrochemical reactions, in which the electrolytes are perturbed from equilibrium. To investigate the influence of the co-salt anion with Li^+ as the

cation, two different electrochemical configurations were compared: (1) Discharge in two-electrode cells with a Li metal anode and Vulcan carbon-based cathode, for suitable comparison with previous results;[25] and (2) A three-electrode electrolysis-type cell containing a Super P carbon - coated glassy carbon working electrode, a fritted $Ag/AgNO_3$ reference electrode and a fritted Pt counter electrode (see SI for additional details). In both setups, following electrolyte preparation, CO_2 introduction, and resting (20 hours), the solutions were re-saturated with CO_2 prior to each measurement to ensure a CO_2 headspace. The three-electrode setup was particularly useful in later measurements to enable comparison across different cations, where stable metal anode analogues to Li are not available.

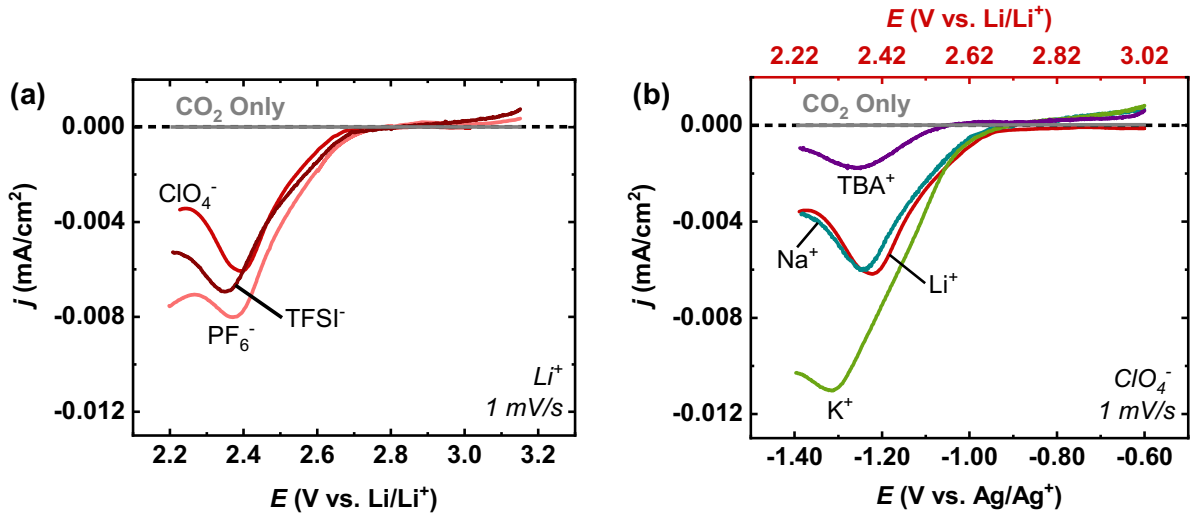

Figure 6: Comparison of capacitance- and *iR*-corrected linear sweep voltammograms at 1 mV/s in 3-electrode measurements with 0.1 M EEA-CO_2 and (a) 0.3 M LiY/DMSO (Y^- = ClO_4^-, PF_6^-, or $TFSI^-$) or (b) 0.3 M $AClO_4$ (A^+ = Li^+, Na^+, K^+ or TBA^+). The top axis in **Figure 6b** displays the potential vs. Li/Li^+ for the scan corresponding to $LiClO_4$ to facilitate comparison with prior galvanostatic results in Li cells. The working electrode in all cases was a super P-coated glassy carbon electrode, and current densities were normalized to the glassy carbon geometric surface area (0.196 cm^2).

Electrochemical measurements on the equilibrated solutions revealed almost identical behavior for all Li-based salts, regardless of the anion. Under galvanostatic discharge conditions in two-electrode cells, nearly identical voltage plateaus (~2.85 V vs. Li/Li^+) and capacities (> 3400 mAh/g_c) were observed (**Figure S10**) at a fixed rate of 20 mA/g_c. The nearly-identical redox potentials confirm that the anion chemistry factors little in the overall free energy change during conversion, and therefore that the anion's participation is weak or negligible in the overall

electrochemical reaction. The comparable capacities reflect that the cell performance was limited by the formation of similar quantities of passivating Li_2CO_3 during discharge.[25] Similar findings were obtained with linear sweep voltammetry measurements conducted at 1 mV/s in **Figure 6a**. Whereas only capacitive backgrounds were observed for either physically-dissolved CO_2 (no EEA) or lean EEA (no CO_2) in the neat electrolytes (**Figure S11**), solutions containing EEA-CO_2 exhibited an evident redox peak upon the negative scan, with similar reduction current magnitudes obtained at comparable onset reduction potentials across the different anions (2.68, 2.69 and 2.70 V vs. Li/Li$^+$ for ClO_4^-, TFSI$^-$ and PF_6^-, respectively).

Linear sweep voltammetry (LSV) measurements were next conducted with varying cations under the same conditions. As shown in **Figure 6b**, nearly-identical onset potentials (approximately -0.94 V vs. Ag/Ag$^+$) were observed with Li$^+$, Na$^+$ and K$^+$ (all CV background scans are included in **Figure S12**). This suggests that the measured electrochemical potentials at reduction onset, in addition to being largely insensitive to anion as expected, also do not strongly reflect the different strengths of ionic interaction in the alkali carbamates. Note that the expected Nernstian shift in the thermodynamic potential of Reaction 4 due to varying concentrations of initial carbamate is less than 10 mV for the relevant range of carbamate proportions here (approximately 50 mM for Li$^+$, 32 mM for Na$^+$, and 11 mM for K$^+$), and therefore differences in reactant population would not be expected to strongly affect the measurable redox potential.

Although there was negligible variation in onset potential, substantially higher reduction rates were obtained with K$^+$. A larger reduction peak current density (-11.2 μA/cm^2) was obtained with K$^+$ compared to Li$^+$ and Na$^+$ (approximately -6.2 μA/cm^2 for both). The exchange current density was also greatest for K$^+$, as qualitatively determined from Tafel responses shown in **Figure S13** as a function of cation. Although it was not possible to directly characterize the reduction products formed with Na$^+$ and K$^+$ (see Supporting Information), the nearly identical onset potentials suggest that the overall reaction scheme is not altered by the alkali cation; i.e., Reaction 4 is generalizable to Na$^+$ and K$^+$. Interestingly, the EEA-CO_2 adducts were also slightly electrochemically active with TBA$^+$; however, a noticeably lower onset reduction potential (by approximately 80 mV) and peak current density (-1.78 μA/cm^2) were observed in comparison to the alkali cations. The electroactivity observed with TBA$^+$ is consistent with the small fraction of TBA$^+$ carbamate formed (**Figure 4**), although, it is unclear at present what reduction products are formed with TBA$^+$ given the likely inability to form carbonate. Taken together, the combined

NMR, ATR-IR, DFT, and electrochemical results indicate: (1) A clear correlation between harder Lewis acid cations and higher quantities of carbamate formed, which reflects the modulated chemical thermodynamics of the reactant state prior to electrochemical reactions; (2) A prevailing role of softer Lewis acid cations, namely K^+, in amplifying the rate of the reduction reaction. Understanding how the cation's selection may factor into higher reduction currents requires non-thermodynamic treatment of the cation's transport properties to investigate more carefully. Therefore, we next employed molecular dynamics (MD) simulations to investigate the different solvation structures and transport behaviors of alkali cations as they approach, and pair with, an available carbamate in solution, simulating the likely ion-transfer process occurring under electrochemical conditions.

Molecular dynamics simulations of the ion-pairing events under reaction conditions

To elucidate the role of the cation under electrochemical conditions, we used MD simulations to investigate the rate and energetics of dynamic ion-pairing between the alkali cation and carbamate anion, which reflects the relative facility of ion transfer from bulk solution in DMSO to the reaction sphere. Note that ion-pairing comprises two coupled processes: loss of solvent from the cation solvation shell and around the $–COO^-$ in the amine; and concurrent electrostatic pairing of the de-shielded alkali cation and carbamate. Our previous characterization of the reactant state indicates that one alkali cation is already pre-associated with each carbamate molecule at the onset of reduction. However, Reaction 4 indicates that three additional alkali cations are consumed in the reduction reaction. The DFT calculations also indicated that electron transfer alone did not lead to detachment of the CO_2-derived species, supporting the fact that additional ion transfer steps occur to the negatively-charged carbamate. Therefore, we hypothesized that the availability of alkali cations for reaction with $RNHCOO^-$ would be an important factor in determining the electrochemical reaction rates. MD was thus used to model the following reaction in which $RNHCOO^-$ represents a model amine-derived anion:

$$\mathrm{RNHCOO^-_{(solv)}} + \mathrm{A^+_{(solv)}} \rightarrow \mathrm{RNHCOOA_{(solv)}} \quad (6)$$

where (solv) denotes a solvated species in DMSO. Note that $RNHCOO^-$ is simply used here to represent a general anionic form of the amine-CO_2 adduct formed during electrochemical

reactions, which may, in practice, correspond to the anion, dianion, and/or cation-paired variants of these species. The typical computational domain had dimensions of 7 × 7 × 7 nm^3 and contained 2885 DMSO molecules, yielding a simulated density of 1.09 g/cm^3, compared to an experimentally established value of 1.1 g/cm^3 at STP. Twenty alkali cations and $RNHCOO^-$ ions each were added to the computational domain, mimicking the amine concentration of 0.1 M used in experiments. Co-salt anions and ammonium cations were not included to simplify the simulations. The equations of motion were integrated using the Verlet (Leap-Frog) algorithm with a time step of 1 fs and simulation time of 80 ns. Initial unpaired and final paired configurations for Li^+ are shown in **Figure 7a-b**, respectively, with Na^+ and K^+ results in **Figure S14**. For method validation, the coordination numbers (CNs) of alkali cations in bulk DMSO (no amine) were first computed, based on the number of O_{DMSO} in the cation's first solvation shell, as 4.1, 4.8, and 5.2 for Li^+, Na^+, and K^+, respectively (**Figure 7c**), consistent with literature reports (Li^+: 4, Na^+: 5, and K^+: 6).[43-45]

The MD simulations indicated, as expected, that the paired configurations corresponded to partial desolvation of all cations to permit electrostatic association with carbamate. However, both the extent, and the rate, of desolvation varied significantly depending on the cation. Specifically, the pairing kinetics of K^+ with $RNHCOO^-$ are significantly more rapid than with either Li^+ or Na^+. Out of a total of 20 possible pairs, in 80 ns, all 20 ion pairs formed for K^+. Meanwhile, over the same simulation time, only eight pairs formed for Li^+, and three for Na^+ (**Figure 7d**). These rates corresponded to approximately 3, 8, and 13 pairs formed/ns, respectively (**Table S2).** This more rapid pairing is attributed to the weaker solvation strength of K^+ in DMSO, resulting in the larger and faster change in the CN for K^+ (CN change of 0.7, 0.3, and 2.2 for Li^+, Na^+, K^+ respectively after 80 ns, **Figures 7c** and **S15**). To quantify the desolvation kinetics, potential of mean force (PMF) calculations were carried out as a function of center-of-mass separation between A^+ and $-COO^-_{RNHCOO}$ in DMSO. As shown in **Figure S16**, the energy barrier, E_a, to reach the transition state of the ion pairing process (Reaction 6) is the smallest for K^+ (E_a=10.1 kJ/mol), followed by Li^+ (E_a=13.8 kJ/mol) and Na^+ (E_a=15.0 kJ/mol). Together, these results explain why higher reduction currents are obtained with K^+, and suggest, interestingly, that ion-transfer from bulk solution to the amine is rate-determining at moderate overpotentials. Note that even though K^+ pairs with $RNHCOO^-$ most rapidly when the carbamic acid is already deprotonated (as may occur during reaction conditions), it does not imply rapid

initial formation of potassium carbamate, because as discussed earlier, the driving force to deprotonate the acid and form potassium carbamate is the lowest among the three alkali cations investigated. Thus, the beneficial energetics of desolvation and ion pairing would have the greatest effect when the system is perturbed from equilibrium and is in ionic form, i.e., actively undergoing electrochemical reactions where facile supply of cations may be essential to sustain reactions, highly consistent with the experimental observations.

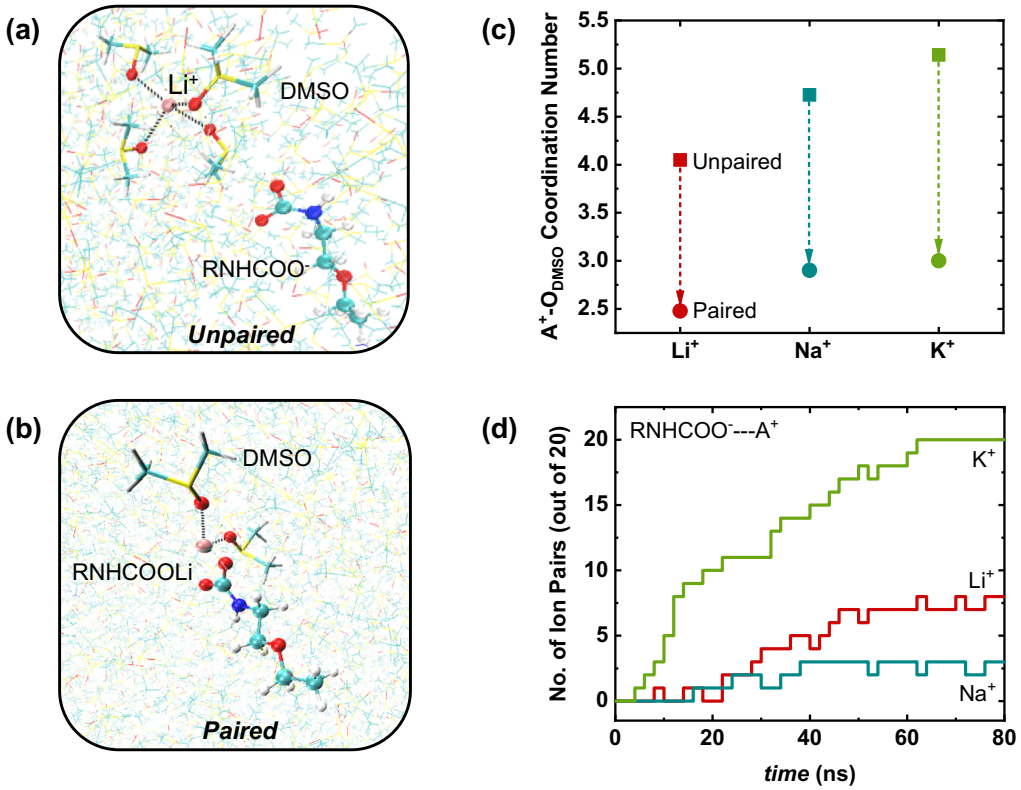

Figure 7: First solvation shell structures for Li^+ in (a) an unpaired configuration, with Li^+ fully solvated by DMSO, and in (b) a paired configuration, with Li^+ electrostatically coordinated to $RNHCOO^-$ following a simulation time of 80 ns. (c) Coordination numbers of the alkali cation, A^+, with DMSO (A^+-O_{DMSO}), computed at equilibrium with all ions initialized in either the unpaired or paired configurations. (d) Number of ion pairs ($RNHCOO^-A^+$) formed as a function of computational time, out of a total of 20 possible pairs.

Taken together, these results provide, first, new and unambiguous evidence that amine-CO_2 adducts exhibit activity in a broader range of added co-salts than known previously. This indicates that the amine-activation process reported in our first work is more generally applicable

than previously understood, opening up the possibility for further development. Second, it reveals mechanistic ways in which the salt does, and does not, play a role. The co-salt cation, and its extended solvation structure, is associated with the adduct prior to electrochemical reactions, and must therefore form a part of the definition of the electroactive reactant state. However, both the reactant state concentration and the identity of the associated alkali cation factor little in the onset reduction potentials, at least for the amine and solvent (EEA/DMSO) examined here. In contrast, the activity at lower potentials is strongly governed by the cation. Our results indicate that this can be explained by the relative availability of bulk ions to react with either carbamate or associated anionic forms, which is favored for K^+, having a weaker solvation strength and lower desolvation barrier. It is interesting to note that Na^+, which lies between Li^+ and K^+ in terms of Lewis acidity, exhibits a linear sweep response and peak current densities that are very similar to that of Li^+, rather than lying in between Li^+ and K^+ (**Figure 6b**). Although elucidating this trend requires further detailed understanding of the electrochemical mechanisms, planned in future work, it is fully consistent with the MD calculations, which indicate that Na^+ has the highest desolvation barrier and therefore cannot sustain high reaction rates due to impeded ion transfer. Overall, our results indicate that coupled ion-transfer is a governing step in the electrochemical reactions of amine-CO_2 adducts in DMSO. Therefore, use of more weakly-solvating solvents in future work may enable higher electrochemical rates to be sustained. In addition, it will be important to identify new amine and solvent combinations with improved bulk transport properties in the CO_2-loaded state. This could support both faster initial rates of CO_2 capture and alkali carbamate (electroactive species) formation, which may also improve electrochemical reaction rates. Amines that undergo weaker intermolecular hydrogen bonding and viscosity changes upon CO_2 loading are currently being developed for CO_2 capture,[46-48] and their suitability for electrochemical reactions should be explored to further support improved capture and conversion rates. If the above limitations can be addressed, the DFT results indicate that further tailoring of amine chemistry to manipulate and optimize N-C bond strength and the overall electronic structure in the EEA-CO_2 adduct may enable finer control over the redox potential and, presumably, the intrinsic electrochemical kinetics.

Conclusions

In summary, these results elucidate the critical role of alkali metal-based co-salts in inducing key shifts in amine-CO_2 adduct speciation, which can be directly linked to subsequent electrochemical activity. Whereas carbamic acids (-COOH) cannot be electrochemically reduced in the absence of free ions, adding electrolyte co-salts yields cation-associated carbamates of EEA that exhibit significantly enhanced electrochemical activity compared to CO_2 only, at potentials in excess of 2.7 V vs. Li/Li^+ or -0.94 vs. Ag/Ag^+ (nonaqueous). The carbamic acid-carbamate equilibria can be modified by altering the electrolyte co-salt cation (Li^+, Na^+, K^+, and TBA^+ investigated herein), with a smaller cation size resulting in increased carbamate formation due to increasing strength of cation – carbamate ionic interactions. Upon electrochemical reduction, however, K^+-paired carbamates show the greatest reduction currents, in spite of the lowest overall population of active carbamates formed. MD simulations reveal that this effect is likely non-thermodynamic in nature, resulting from improved K^+ transfer from bulk solution to the reaction site during electrochemical reduction. Although the full multi-bodied, multi-step reaction mechanisms are complex and require continued examination to elucidate in full, these results indicate that electrochemical reaction rates of amine-CO_2 adducts may be significantly improved by carefully tailoring cation-solvent-amine interactions.

Conflicts of interest

There are no conflicts to declare.

Acknowledgements

This research was supported by startup funding from the MIT Department of Mechanical Engineering. The authors acknowledge the Small Molecule Mass Spectrometry—A Harvard FAS Division of Science Core Facility - for assistance with mass spectrometry measurements. This work made use of the MRSEC Shared Experimental Facilities at MIT, supported by the National Science Foundation under award number DMR-14-19807. L.Z. acknowledges funding from the National Natural Science Foundation of China (Grant No. 51776041) and the China Scholarship Council (201706095025). This work used the Extreme Science and Engineering Discovery Environment (XSEDE)[49] (supported by National Science Foundation grant number ACI-1548562) Comet at the San Diego Supercomputer Center through allocation TG-CTS180040.

Supporting Information

Detailed experimental and computational methods, carbamate quantification calculation from ^{1}H NMR, time-dependent 1H NMR spectra, Karl Fischer measurements for water content determination, linear sweep voltammograms for background (no EEA and no CO_2) cases, Tafel responses, electronic density distribution for carbamates, first solvation shell structures for Na^+ and K^+, rate of change in coordination number, variation in potential of mean force (PMF) upon ion-pairing, and residence time correlation functions.

References

1. Markewitz, P.; Kuckshinrichs, W.; Leitner, W.; Linssen, J.; Zapp, P.; Bongartz, R.; Schreiber, A.; Müller, T. E., Worldwide innovations in the development of carbon capture technologies and the utilization of CO_2. *Energy Environ. Sci.* **2012,** *5* (6), 7281-7305.
2. Hunt, A. J.; Sin, E. H. K.; Marriott, R.; Clark, J. H., Generation, Capture, and Utilization of Industrial Carbon Dioxide. *ChemSusChem* **2010,** *3* (3), 306-322.
3. Appel, A. M.; Bercaw, J. E.; Bocarsly, A. B.; Dobbek, H.; DuBois, D. L.; Dupuis, M.; Ferry, J. G.; Fujita, E.; Hille, R.; Kenis, P. J. A. et al., Frontiers, Opportunities, and Challenges in Biochemical and Chemical Catalysis of CO_2 Fixation. *Chem. Rev.* **2013,** *113* (8), 6621-6658.
4. Whipple, D. T.; Kenis, P. J. A., Prospects of CO_2 Utilization via Direct Heterogeneous Electrochemical Reduction. *J. Phys. Chem. Lett.* **2010,** *1* (24), 3451-3458.
5. Boot-Handford, M. E.; Abanades, J. C.; Anthony, E. J.; Blunt, M. J.; Brandani, S.; Mac Dowell, N.; Fernández, J. R.; Ferrari, M.-C.; Gross, R.; Hallett, J. P. et al., Carbon capture and storage update. *Energy Environ. Sci.* **2014,** *7* (1), 130-189.
6. Aaron, D.; Tsouris, C., Separation of CO_2 from Flue Gas: A Review. *Sep. Sci. Technol.* **2005,** *40* (1-3), 321-348.
7. Hong, W. T.; Risch, M.; Stoerzinger, K. A.; Grimaud, A.; Suntivich, J.; Shao-Horn, Y., Toward the rational design of non-precious transition metal oxides for oxygen electrocatalysis. *Energy Environ. Sci.* **2015,** *8* (5), 1404-1427.
8. Walter, M. G.; Warren, E. L.; McKone, J. R.; Boettcher, S. W.; Mi, Q.; Santori, E. A.; Lewis, N. S., Solar Water Splitting Cells. *Chem. Rev.* **2010,** *110* (11), 6446-6473.
9. Benson, E. E.; Kubiak, C. P.; Sathrum, A. J.; Smieja, J. M., Electrocatalytic and homogeneous approaches to conversion of CO_2 to liquid fuels. *Chem. Soc. Rev.* **2009,** *38* (1), 89-99.
10. Gattrell, M.; Gupta, N.; Co, A., A review of the aqueous electrochemical reduction of CO_2 to hydrocarbons at copper. *J. Electroanal. Chem.* **2006,** *594* (1), 1-19.
11. Machado, A. S. R.; da Ponte, M. N., CO_2 capture and electrochemical conversion. *Curr. Opin. Green Sustainable Chem.* **2018,** *11*, 86-90.
12. Yang, Z. Z.; Zhao, Y. N.; He, L. N., CO_2 chemistry: task-specific ionic liquids for CO_2 capture/activation and subsequent conversion. *Rsc Adv* **2011,** *1* (4), 545-567.
13. Arti, M.; Youn, M. H.; Park, K. T.; Kim, H. J.; Kim, Y. E.; Jeong, S. K., Single Process for CO_2 Capture and Mineralization in Various Alkanolamines Using Calcium Chloride. *Energy Fuels* **2017,** *31* (1), 763-769.

14. Luca, O. R.; Fenwick, A. Q., Organic reactions for the electrochemical and photochemical production of chemical fuels from CO_2 - The reduction chemistry of carboxylic acids and derivatives as bent CO_2 surrogates. *J. Photochem. Photobiol. B* **2015,** *152*, 26-42.
15. Luca, O. R.; McCrory, C. C. L.; Dalleska, N. F.; Koval, C. A., The Selective Electrochemical Conversion of Preactivated CO_2 to Methane. *J. Electrochem. Soc.* **2015,** *162* (7), H473-H476.
16. Kuhl, K. P.; Cave, E. R.; Abram, D. N.; Jaramillo, T. F., New insights into the electrochemical reduction of carbon dioxide on metallic copper surfaces. *Energy Environ. Sci.* **2012,** *5* (5), 7050-7059.
17. Chen, L.; Li, F.; Zhang, Y.; Bentley Cameron, L.; Horne, M.; Bond Alan, M.; Zhang, J., Electrochemical Reduction of Carbon Dioxide in a Monoethanolamine Capture Medium. *ChemSusChem* **2017,** *10* (20), 4109-4118.
18. McCann, N.; Maeder, M.; Attalla, M., Simulation of Enthalpy and Capacity of CO_2 Absorption by Aqueous Amine Systems. *Ind. Eng. Chem. Res.* **2008,** *47* (6), 2002-2009.
19. Kim, I.; Svendsen, H. F., Heat of Absorption of Carbon Dioxide (CO_2) in Monoethanolamine (MEA) and 2-(Aminoethyl)ethanolamine (AEEA) Solutions. *Ind. Eng. Chem. Res.* **2007,** *46* (17), 5803-5809.
20. Svensson, H.; Zejnullahu Velasco, V.; Hulteberg, C.; Karlsson, H. T., Heat of absorption of carbon dioxide in mixtures of 2-amino-2-methyl-1-propanol and organic solvents. *Int. J. Greenhouse Gas Control* **2014,** *30*, 1-8.
21. Gurkan, B. E.; de la Fuente, J. C.; Mindrup, E. M.; Ficke, L. E.; Goodrich, B. F.; Price, E. A.; Schneider, W. F.; Brennecke, J. F., Equimolar CO_2 Absorption by Anion-Functionalized Ionic Liquids. *J. Am. Chem. Soc.* **2010,** *132* (7), 2116-2117.
22. Rochelle, G. T., Amine scrubbing for CO2 capture. *Science* **2009,** *325* (5948), 1652-4.
23. Heldebrant, D. J.; Koech, P. K.; Glezakou, V. A.; Rousseau, R.; Malhotra, D.; Cantu, D. C., Water-Lean Solvents for Post-Combustion CO_2 Capture: Fundamentals, Uncertainties, Opportunities, and Outlook. *Chem. Rev.* **2017,** *117* (14), 9594-9624.
24. Seo, S.; Quiroz-Guzman, M.; DeSilva, M. A.; Lee, T. B.; Huang, Y.; Goodrich, B. F.; Schneider, W. F.; Brennecke, J. F., Chemically Tunable Ionic Liquids with Aprotic Heterocyclic Anion (AHA) for CO_2 Capture. *J. Phys. Chem. B* **2014,** *118* (21), 5740-5751.
25. Khurram, A.; He, M.; Gallant, B. M., Tailoring the Discharge Reaction in Li-CO2 Batteries through Incorporation of CO_2 Capture Chemistry. *Joule* **2018,** *2* (12), 2649-2666.
26. Amatore, C.; Saveant, J. M., Mechanism and kinetic characteristics of the electrochemical reduction of carbon dioxide in media of low proton availability. *J. Am. Chem. Soc.* **1981,** *103* (17), 5021-5023.
27. Yang, S. X.; Qiao, Y.; He, P.; Liu, Y. J.; Cheng, Z.; Zhu, J. J.; Zhou, H. S., A reversible lithium-CO_2 battery with Ru nanoparticles as a cathode catalyst. *Energy Environ. Sci.* **2017,** *10* (4), 972-978.
28. Bishnoi, S.; Rochelle, G. T., Absorption of carbon dioxide into aqueous piperazine: reaction kinetics, mass transfer and solubility. *Chem. Eng. Sci.* **2000,** *55* (22), 5531-5543.
29. Farrokhpour, H.; Manassir, M., A Simple Method for Estimating the Absolute Solvation Free Energy of Monovalent Ions in Different Solvents. *J. Phys. Chem. A* **2015,** *119* (1), 160-171.

30. Marenich, A. V.; Cramer, C. J.; Truhlar, D. G., Universal Solvation Model Based on Solute Electron Density and on a Continuum Model of the Solvent Defined by the Bulk Dielectric Constant and Atomic Surface Tensions. *J. Phys. Chem. B* **2009,** *113* (18), 6378-6396.
31. Van Der Spoel, D.; Lindahl, E.; Hess, B.; Groenhof, G.; Mark Alan, E.; Berendsen Herman, J. C., GROMACS: Fast, flexible, and free. *J. Comput. Chem.* **2005,** *26* (16), 1701-1718.
32. Strader, M. L.; Feller, S. E., A Flexible All-Atom Model of Dimethyl Sulfoxide for Molecular Dynamics Simulations. *J. Phys. Chem. A* **2002,** *106* (6), 1074-1080.
33. Jorgensen, W. L.; Maxwell, D. S.; Tirado-Rives, J., Development and Testing of the OPLS All-Atom Force Field on Conformational Energetics and Properties of Organic Liquids. *J. Am. Chem. Soc.* **1996,** *118* (45), 11225-11236.
34. Kortunov, P. V.; Siskin, M.; Baugh, L. S.; Calabro, D. C., In Situ Nuclear Magnetic Resonance Mechanistic Studies of Carbon Dioxide Reactions with Liquid Amines in Non-aqueous Systems: Evidence for the Formation of Carbamic Acids and Zwitterionic Species. *Energy & Fuels* **2015,** *29* (9), 5940-5966.
35. Kortunov, P. V.; Siskin, M.; Baugh, L. S.; Calabro, D. C., In Situ Nuclear Magnetic Resonance Mechanistic Studies of Carbon Dioxide Reactions with Liquid Amines in Aqueous Systems: New Insights on Carbon Capture Reaction Pathways. *Energy & Fuels* **2015,** *29* (9), 5919-5939.
36. Andreoni, W.; Pietrucci, F., CO_2 capture in amine solutions: modelling and simulations with non-empirical methods. *J. Phys.: Condens. Matter* **2016,** *28* (50), 503003.
37. García-Abuín, A.; Gomez-Díaz, D.; Lopez, A. B.; Navaza, J. M.; Rumbo, A., NMR characterization of carbon dioxide chemical absorption with monoethanolamine, diethanolamine, and triethanolamine. *Ind. Eng. Chem. Res.* **2013,** *52* (37), 13432-13438.
38. Becke, A. D., Perspective: Fifty years of density-functional theory in chemical physics. *J, Chem. Phys.* **2014,** *140* (18), 18A301.
39. Richner, G.; Puxty, G., Assessing the Chemical Speciation during CO_2 Absorption by Aqueous Amines Using in Situ FTIR. *Ind. Eng. Chem. Res.* **2012,** *51* (44), 14317-14324.
40. Jackson, P.; Robinson, K.; Puxty, G.; Attalla, M., In situ Fourier Transform-Infrared (FT-IR) analysis of carbon dioxide absorption and desorption in amine solutions. *Energy Procedia* **2009,** *1* (1), 985-994.
41. Robinson, K.; McCluskey, A.; Attalla Moetaz, I., An FTIR Spectroscopic Study on the Effect of Molecular Structural Variations on the CO_2 Absorption Characteristics of Heterocyclic Amines. *ChemPhysChem* **2011,** *12* (6), 1088-1099.
42. Bhugun, I.; Lexa, D.; Savéant, J.-M., Catalysis of the Electrochemical Reduction of Carbon Dioxide by Iron(0) Porphyrins. Synergistic Effect of Lewis Acid Cations. *The Journal of Physical Chemistry* **1996,** *100* (51), 19981-19985.
43. Westphal, E.; Pliego, J. R., Absolute solvation free energy of Li^+ and Na^+ ions in dimethyl sulfoxide solution: A theoretical ab initio and cluster-continuum model study. *J. Chem. Phys.* **2005,** *123* (7), 074508.
44. Guchik, I. V.; Frolov, Y. L.; Shagun, V. A.; Vashchenko, A. V.; Trofimov, B. A., Quantum-Chemical Analysis of Coordination of Dimethylsulfoxide Molecules to Sodium and Potassium Cations. *J. Struct. Chem.* **2004,** *45* (1), 41-46.

45. Siddique, A. A.; Dixit, M. K.; Tembe, B. L., Solvation structure and dynamics of potassium chloride ion pair in dimethyl sulfoxide–water mixtures. *Journal of Molecular Liquids* **2013,** *188*, 5-12.
46. Malhotra, D.; Koech, P. K.; Heldebrant, D. J.; Cantu, D. C.; Zheng, F.; Glezakou, V.-A.; Rousseau, R., Reinventing Design Principles for Developing Low-Viscosity Carbon Dioxide-Binding Organic Liquids for Flue Gas Clean Up. *ChemSusChem* **2017,** *10* (3), 636-642.
47. Cantu, D. C.; Lee, J.; Lee, M.-S.; Heldebrant, D. J.; Koech, P. K.; Freeman, C. J.; Rousseau, R.; Glezakou, V.-A., Dynamic Acid/Base Equilibrium in Single Component Switchable Ionic Liquids and Consequences on Viscosity. *J. Phys. Chem. Lett.* **2016,** *7* (9), 1646-1652.
48. Luo, X. Y.; Fan, X.; Shi, G. L.; Li, H. R.; Wang, C. M., Decreasing the viscosity in CO_2 capture by amino-functionalized ionic liquids through the formation of intramolecular hydrogen bond. *J. Phys. Chem. B* **2016,** *120* (10), 2807-2813.
49. Towns, J.; Cockerill, T.; Dahan, M.; Foster, I.; Gaither, K.; Grimshaw, A.; Hazlewood, V.; Lathrop, S.; Lifka, D.; Peterson, G. D.; Roskies, R.; Scott, J. R.; Wilkins-Diehr, N., XSEDE: Accelerating Scientific Discovery. *Computing in Science & Engineering* **2014,** *16* (5), 62-74.

TOC Graphic:

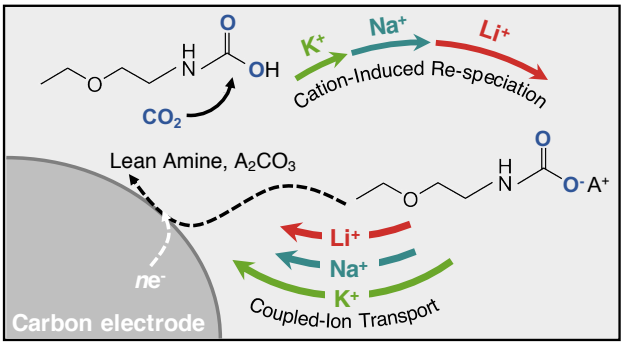
K+
Na+
Li+
Cation-Induced Re-speciation
CO2
Lean Amine, A2CO3
Li+
Na+
K+
Coupled-Ion Transport
ne-
Carbon electrode